ScienSage

Journal of Advanced Scientific Research

Available online through http://www.sciensage.info

ISSN
0976-9595
Research Article

ANALYSIS OF MOLECULAR STRUCTURE, VIBRATIONAL SPECTRA, ELECTRONIC PROPERTIES AND MOLECULAR DOCKING STUDIES OF GENKWANIN AS POTENT CYCLOOXYGENASE ENZYMES INHIBITOR

A. Harikrishnan*[1], R. Madivanane[2]

[1]*Department of Physics, Bharathiar University, Coimbatore, Tamilnadu, India*

[2]*Department of Physics, Bharathidasan Govt College for Women, Puducherry, India*

**Corresponding author: krishhari80@yahoo.co.in*

ABSTRACT

In the present study, the optimized geometrical parameters and vibrational frequencies of the Genkwanin (5-hydroxy-2-(4-hydroxyphenyl)-7- methoxychromen-4-one) were obtained by both hatree fock(HF) and density functional theory(DFT) methods. The experimental FT-IR, FT-Raman spectrum of the compound has been recorded in the region 4000-600cm^{-1} and 50-4000cm^{-1} respectively. The calculated structural parameters and vibrational frequencies were analyzed and compared with obtained experimental results. The frontier molecular orbital (FMO), molecular electrostatic potential (MEP) and UV-vis studies of the compound has been computed to elucidate the electronic properties. Moreover, molecular docking studies were also carried out to investigate the inhibitory effect of the compound against cyclooxygenase (COX) enzymes. Results of molecular docking study reveals that the chosen compound effectively inhibits the active sites of the human cyclooxygenase(COX-1 and COX-2) enzyme. The binding energy of the compound were studied and compared to standard drugs Ibuprofen, Nimesulide and Mefenamic acid. The investigated compound showed good binding affinity compared to standard drugs. Therefore, this study is an attempt to identify a safe and effective new drug from flavonoids for the treatment of inflammatory disease.

Keywords: Genkwanin, Cyclooxygenase, Molecular docking, Anti-Inflammatory

1. INTRODUCTION

At present, a strong interest is concentrated in the natural compounds and has developed in recent years as a consequence of drug costs and safety in numerous disease conditions. Looking at the present state of affairs, Flavonoids are an admirable lead compounds to develop efficient, affordable, good therapeutic index [1]. In the present study, we have made an attempt to analyze the nature of structure, functional groups, vibrational frequencies, chemically active sites and possible binding affinity of the flavonoid Genkwanin(GKW) using a quantum chemical and molecular docking approach. GKW is a widely available bioactive and non-glycosylated flavonoid which is isolated from GenkwaFlos (Daphne Genkwa Sieb.et Zucc.) and rosemary (*Rosmarinusocinalis L.)*[. 2]GKW shows a remarkable pharmacological efficiency such as anti-inflammatory [3], radical scavenging activitie [4], chemo preventive [5], antibacterial [6] and antiplasmodial [7]. An *in-vitro* study reveals that nanosuspension of GKW exhibit a potent anti-tumor activity and good tolerance against human tumor cell lines [8, 9]. Recently, quantum chemical computations, combined with FTIR/ FT-Raman spectroscopy has been used as an effective tool in the biological compounds [10], and vibrational analysis of drug molecules [11]. As far as we know, there is no FTIR, FT-Raman and quantum chemical spectroscopic investigation on GKW in the literature. Due to the wide range of pharmacological properties of the GKW, an attempt has been made in this study to report a complete analysis of structural parameters and vibrational assignments of GKW by combining experimental FT-IR, FT-Raman spectroscopic and quantum chemical calculations methods. In order to understand the interaction energy between the two molecules and the behavior of small molecules in the binding site of target proteins, molecular docking studies were also carried out. The binding mechanism of GKW with various cyclooxygenase(COX and COX-2) enzymes and their binding energies, inter-molecular hydrogen bond interaction were also studied and compared with the standard non-steroidal anti-inflammatory drugs (NSAIDs).

2. MATERIAL AND METHOD

2.1. Computational Details

The molecular geometrical parameters of GKW were computed in the ground state by performing both HF and DFT (B3LYP) with 6-311++G (d,p) basis sets. For the optimized structure (Fig.1), frontier molecular orbital (HOMO-LUMO) and molecular electrostatic potential surface were computed at DFT/B3LYP with 6-311++G (d,p) basis set level of theory to identify the electron density transfer and reactive sites of the compound respectively. Theoretical Ultraviolet-visible (UV) spectrum of the title molecule has also been calculated using TD-DFT methods. All the theoretical calculations were carried out with Gaussian 09 software program [12] together with Gauss view visualization program [13] with the default convergence criteria. No symmetry restriction has been set for all the optimizations. VEDA4 program [14] has been used to calculate potential energy distribution (PED) for each of the vibrational frequencies. The vibrational assignments have also been assigned by combining the results of the potential energy distribution and Gauss view program.

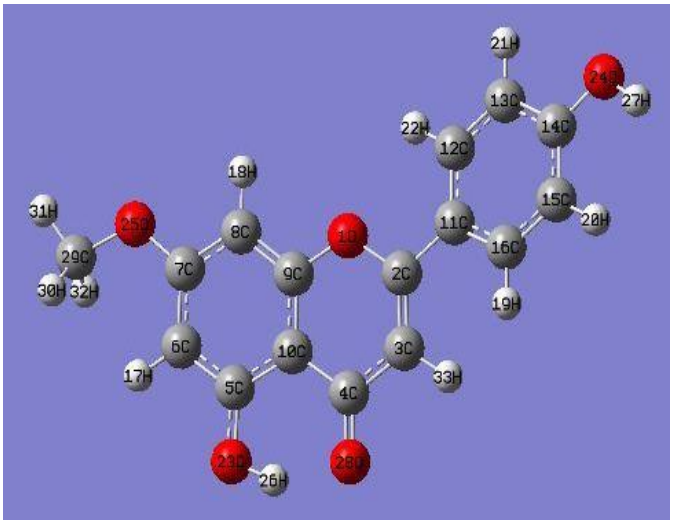

Fig. 1: Optimized molecular structure of GKW

2.2. Experimental Details

The compound under investigation was purchased from ChemFaces (Wuhan Economic and Technological Development Zone Hube, China) with a assay of 98% and was utilized for recording FT-IR and FT-Raman spectra without any further purification. The FTIR spectra of the compound has been recorded in the 4000-600cm^{-1} region at the spectral resolution of 4cm^{-1} using Cary 630 FTIR spectrometer out-fitted with attenuated total reflectance sampling interface (Agilent Technologies, USA). The Cary 630 MicroLab PC computer programs were used to collect in- formation and Agilent Resolution Pro writing computer programs were utilized to investigate the information. The FT-Raman spectrum of the compound was also recorded utilizing BRUKER RFS 27: Stand alone FT-Raman Spectrometer with Nd: YAG laser source operating in the region 50-4000cm^{-1} at 1.064 nm line widths with 200 mW powers. The experimental and simulated FTIR and FT-Raman spec tra of GKW are shown in Fig. 1 and 2.

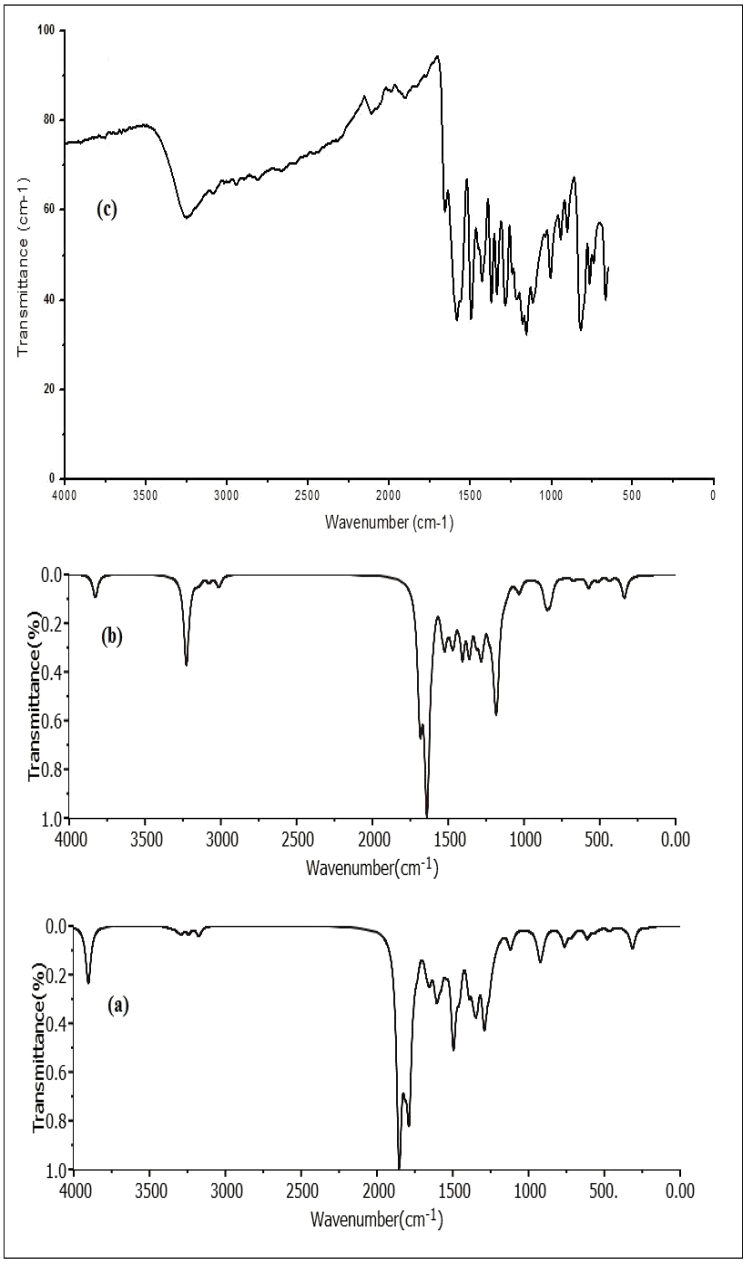

Fig. 2: (a) HF- simulated FTIR (b) DFT/B3LYP - simulated FTIR (c) Experimental FTIR spectrum

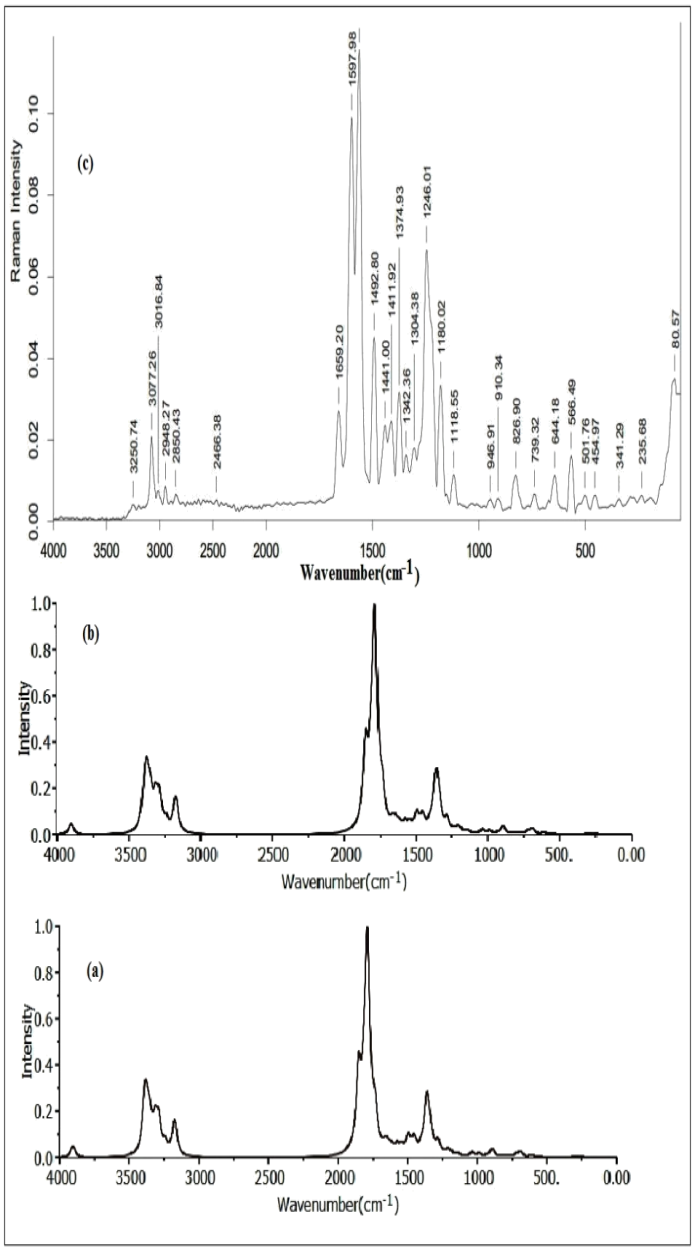

Fig. 3: (a) HF- simulated FT-Raman, (b) DFT/B3LYP - simulated FT-Raman, (c) Experimental FT-Raman spectrum

3. RESULTS AND DISCUSSION

3.1. Molecular geometry analysis

In general, flavonoids consist of two different regions; benzopyrone (A and C) ring and phenyl ring (B). The benzopyrone ring including the hydroxyl and carbonyl groups lie in one plane and the phenyl ring (B) lie on the other plane. Molecular geometries of the GKW were fully optimized by Bernys optimization algorithm using redundant internal co-ordinates. At the optimized structures of GKW, no imaginary frequencies were encountered proving that the potential energy of the optimized structure was minimum. The selected optimized geometrical parameters of GKW are presented in Table 1. To the best of our knowledge, no X-ray crystallographic data of the GKW has yet been established. However, the theoretical results are compared with crystal structure of structurally similar molecule 4, 5-Dihydroxy-7- methoxyflavanone [15]. From the table 1, it was found that the bond lengths and bond angles computed at B3LYP methods are more consistent with the experimental values than the HF method. The C2-C11 bond connects the phenyl and chromone ring with distance of 1.470Å in DFT and 1.477Å in HF is shorter than the assigned bond length 1.501Å due to the double bond nature of the C2=C3. Moreover, this bond length is acceptable when compared with literature values 1.470Å [16] and 1.474Å [17]. The parameters of the hydrogen atoms which are bonded to the atoms O23, O24 are in the range 0.941-0.954Å in HF, 0.963-0.994Å in DFT and 0.750-0.820Å in the crystal. Furthermore, the bond lengths of all other H atoms which are bonded to ring with the C-H are in the range 1.070-1.077Å in HF, 1.080-1.086Å in DFT and is observed in the range of 0.930Å in the crystal structure. It is noteworthy that a strong intra-molecular hydrogen bond interaction (O23-H26----O28) is observed between the hydroxyl group at C5 on the A-ring and the 4-keto group(C=O) in the C-ring. This kind of intra-molecular hydrogen bond interaction has been extensively studied for similar compound those posses hydroxyl group at C5 position [18]. The calculated intra-molecular hydrogen bond (H26-O28) at *Ab initio* HF and DFT/B3LYP are 1.700Å and 1.835Å respectively and this similar result were also observed at 1.900Å in the crystal structure. This strong intra-molecular hydrogen bond results in a six-member ring which is coplanar to benzopyrone ring (A and B) and stabilizes the structure. Due to this intra-molecular hydrogen bond interaction (O23-H26-----O28), an elongation is observed in the bond length of O23-H26 than the other hydroxyl group O24-H27. Also, a smaller bond angle (C5-O23-H26 = 106.8) is observed compared to the other bond angle. Owing to the substitution of carbonyl group at C4, the bond length of C3-C4 and C4-C10 are increased and the bond angle C3-C4-C10 is contracted to 115.02. The substitution of electron donating methoxy group at C7 leads to a deviation of the internal angles (C6-C7-C8) to 121.4^{o}.

Table 1. Selected optimized geometric parameters of GKW

Bond Length(A°)	HF	DFT	Exp [15]	Bond Angle(A°)	HF	DFT	Exp [15]
O1-C2	1.341	1.361	1.465	C2-O1-C9	121.7	120.8	115.3
O1-C9	1.350	1.373	1.365	O1-C2-C3	122.2	121.7	109.5
C2-C11	1.477	1.470	1.501	O1-C2-C11	112.0	112.2	107.3
C3-C4	1.454	1.446	1.511	C3-C2-C11	125.8	126.1	115.3
C3-H33	1.070	1.080	0.970	C3-C4-C10	114.8	115.2	116.3
C4-C10	1.458	1.453	1.437	C6-C7-C8	121.3	121.4	120.8
C4-O28	1.212	1.249	1.252	C5-O23-H26	109.7	106.8	109.5
C5-O23	1.323	1.339	1.364	O25-C29-H30	111.2	111.2	109.5
C6-H17	1.071	1.080	0.930	O25-C29-H31	105.9	105.6	109.5
C7-O25	1.333	1.357	1.361	O25-C29-H32	111.2	111.3	109.5
C8-H18	1.072	1.081	0.930	**Dihedral Angle(A°)**	**HF**	**DFT**	**Exp[15]**
C12-H22	1.073	1.082	0.930	C9-O1-C2-C11	179.6	179.5	-
C13-H21	1.074	1.083	0.930	C2-O1-C9-C8	-179.6	-179.7	-
C14-O24	1.345	1.363	1.369	O1-C2-C11-C12	-23.9	-18.0	-
O23-H26	0.954	0.994	0.820	C6-C5-O23-H26	179.9	179.9	-
O24-H27	0.941	0.963	0.750	C10-C5-O23-H26	-0.1	-0.1	-
O25-C29	1.405	1.425	1.435	C6-C7-O25-H29	0.1	0.3	-
H26-O28	1.835	1.700	1.900	C8-C7-O25-H29	-179.9	-179.7	-
C29-H30	1.085	1.094	0.960	O13-C14-C24-H27	-179.7	-180.0	-

Furthermore, the computed bond angles C3-C2-C11, C3-C2-O1 and C11-C2-O1 are somewhat dispersed with the experimental values due to slight twist between the phenyl ring (B) and benzopyrone ring (A and B). The calculated dihedral angle C3- C2-C11-C16 and O1-C2-C11-C12 between the benzopyrone and the phenyl ring are -1.2^o and 177.7^o respectively. Due to the steric hindrance and repulsion between the benzopyrone and phenyl ring, the later is slightly deviated from the plane of the former and it is evident from the HF and DFT study.

3.2. Vibrational analysis

The geometry of GKW under investigation consists of 33 atoms and 96 normal modes of vibration by possessing C1 point group symmetry. The selected vibrational frequencies calculated at HF and B3LYP methods with 6-311++G (d, p) basis set along with their assignments are summarized in Table 2 (PED values less than 10% are not shown). There are slight disagreements between calculated and observed wave numbers because of the combination of electron correlation effects, basis set of deficiencies and consequence of the anharmonicity. Besides, the theoretical calculations were made for a free molecule in vacuum, while the experiments were performed for the solid sample. It is a general tendency of the quantum mechanical method to overestimate the wave numbers at the exact equilibrium geometry. Therefore, it is customary to scale down the computed harmonic frequencies to improve the agreement between the theoretical and experimental wave numbers. The calculated vibrational frequencies are scaled with a scaling factor 0.99, 0.98, 0.97 [19]. The scaled frequencies are in good agreement with the observed ones. The vibrational frequency assignments have been assigned based on the detailed motion of the individual atoms by using the GAUSSVIEW program and the potential energy distribution values calculated by VEDA4 program. In a five or six member ring system, if the hydroxyl group involves intra- molecular hydrogen bonding it would lower the OH stretching wave number in the region between 3550-3200cm^{-1}. On the other hand, the hydroxyl group which is not involved in intra-molecular hydrogen bonding can absorb strongly in the region 3600-3500cm^{-1} [17].

Accordingly, a strong intra- molecular hydrogen bond O23- H26—-O28 is observed in the present molecule and therefore the band calculated at 3830cm^{-1} in DFT with PED of 100% is assigned to OH stretching vibration. The absorbing band found at 3250cm^{-1} in both FT-IR and FT-Raman spectra is also assigned to the OH stretching vibration and this assignment is well supported by the DFT value at 3198cm^{-1} with PED contribution of

95%. In an aromatic ring system, the C-H stretching vibrations are observed in the region 3100-3000cm^{-1} [16] while the same vibration is also lie in the region 2975-2840cm^{-1} in the methyl group [20]. The bands computed at 3212cm^{-1} in HF and 3049cm^{-1} in B3LYP method are assigned to C-H stretching vibrations for aromatic ring system and the corresponding experimental values are 3088cm^{-1} in FTIR and 3077cm^{-1} in FT-Raman. The bands appeared at 3016cm^{-1} in FT-Raman and 2986cm^{-1} in B3LYP are also assigned to C-H ring stretching vibrations in the methoxy group. For 4,5,7-trihydroxyavone (Naringenin), the C=O stretching vibrational band is observed at 1658cm^{-1} in the FTIR and 1660cm^{-1} in FT-Raman [21].

Table 2: Selected experimental and calculated vibrational frequencies and assignments of GKW

Experimental Frequencies (Cm^{-1})		Calculated Frequencies (Cm^{-1}) with 6-311G++(d,p) basis set				Vibrational Assignments (PED %)
FTIR	FTR	HF Unscaled	DFT Unscaled	HF Scaled	DFT Scaled	
-	-	4183	3830	4140	3792	υs OH(100)
3250	3250	3907	3230	3868	3198	υs OH(95)
3088	3077	3244	3080	3212	3049	υs CH(99)
-	3016	3177	3016	3146	2986	υs CH(81)
1657	1659	1819	1657	1801	1641	υas C=O(27)
1584	1597	1739	1603	1721	1587	υs CC(27)
-	1562	1677	1544	1660	1528	υs CC(11)
1495	1492	1622	1493	1606	1478	β HCH(38)
1429	1441	1546	1436	1531	1422	υas CC(13)
-	1411	1498	1409	1483	1395	υs CC(24)
1371	1374	1463	1370	1448	1356	υs CC(13)
1337	1342	1405	1342	1391	1329	υs CC(46)
-	1304	1397	1318	1383	1305	υs CC(12)
1285	-	1361	1284	1348	1272	υas CC(21)
1242	1246	1337	1235	1324	1223	β HCC(23)
1216	-	1296	1212	1283	1200	β HCC(27)
1178	1180	1262	1178	1250	1166	β HCC(18)
1156	-	1237	1166	1225	1154	β HCH(12)
1116	1118	1192	1115	1180	1104	υs OC(37)
1006	-	1098	982	1087	972	τHCCC (35)
944	946	1043	953	1032	944	τCCCO(12)
903	910	991	919	981	910	β CCO(16)
-	826	896	824	887	815	γOCCC (11)
819	-	838	816	830	808	τHCCC (32)
765	-	809	750	801	742	γOCCC (14)
741	-	793	745	785	738	γOCCC (18)
-	739	767	737	759	729	γCCOC (18)
667	-	726	666	718	659	γCCOC (23)
-	644	700	646	693	640	γCCOC (47)
-	566	614	574	608	568	β OCC(16)
-	501	534	501	528	496	β CCC(16)
-	454	474	446	469	442	β OCC(11)
-	341	348	340	345	336	τHOCC (49)
-	235	245	232	242	230	τHOCC (19)
-	80	75	74	75	73	β COC(10)

υs - symmetric stretching, υas- asymmetric stretching, β- in-plane-bending, γ - out-of-plane bending, τ – Torsion. Potential energy distribution (PED); values less than 10% are not shown.

In the present study, the same C=O stretching vibration is observed at 1657cm^{-1} in Infrared spectra, 1659cm^{-1} in Raman spectra and the same was calculated at 1641cm^{-1} in B3LYP method. The calculated remaining modes of vibration are presented as combinations of the various contributions and the vibrational wavenumbers are very well coincide with the literature [22].

3.3. Frontier molecular orbital(FMO) analysis

Transition of electron is due to interaction between HOMO and LUMO of reacting species, therefore the HOMO - LUMO of the chemical species are very important in defining organic compounds reactivity [23]. A highest occupied molecular orbital having high value of Energy (E_{HOMO}) is likely has a tendency to donate electrons to appropriate acceptor of low empty molecular orbital energy. The HOMO-LUMO gap is an important stability index; the smaller HOMO-LUMO gap indicates less stability, more polarizable, easier the electron transition and is generally associated with a high chemical reactivity, low kinetic stability [24]. The high value of E_{HOMO}-E_{LUMO} is likely indicates low chemical reactivity and high stability. The HOMO and LUMO of GKW computed at B3LYP method is as shown in Fig. 4.

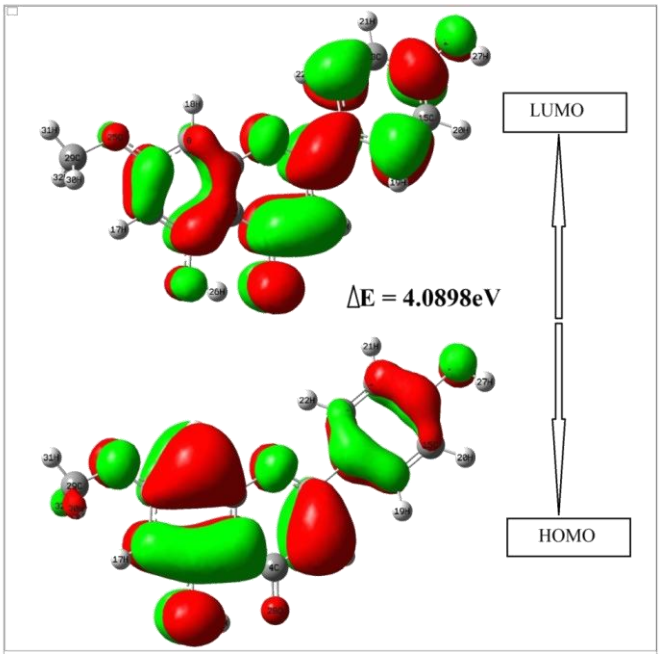

Fig. 4: The HOMO - LUMO of GKW computed at B3LYP method

Due the presence of the C2-C3 double bond in the studied molecule, the eventual charge transfer interactions taking place HOMO to LUMO and the charge delocalization spreading from A to B ring through the C one. The LUMO is delocalized over the entire C-C and C-O bond whereas the HOMO is localized over on all groups. The energy of the highest occupied molecular orbital (E_{HOMO}) and the lowest unoccupied molecular orbital (E_{LUMO}) of the investigated compound is 6.2047 eVand 2.1148 eV respectively. As a result, the energy gab of the compound is about 4.0898 eV.

3.4. UV-visible studies and Electronic properties analysis

Based on the previously optimized ground-state geometry of the molecule, The low energy electronic excited states of the GKW are calculated with the solvent of methanol, at the B3LYP/6-311++G (d,p) level using the TD-DFT approach. The calculated results involving the excitation energies, oscillator strengths (f) and absorption wavelengths were compared with the measured experimental data [25]. All the theoretical parameters computed along with experimental absorption wavelengths are presented in Table 3. It is evident that the experimentally measured wavelengths are close to the computed results. The UV spectrum of the flavonoid typically consists of two absorption maxima, band I conjugated with the rings B and C in the ranges of 300-550 nm and band II conjugated with the ring A and its substitution in the ranges of 240-285nm [26]. The strong absorption peak calculated at 350.67 nm and the corresponding measured wavelength 333 nm is caused by the pi–pi* transitions and the other weak bands assigned at 313.44(3.9556 eV) and 295.20(4.2000eV) nm are due to n-p transition. In view of calculated absorption spectra, the maximum absorption wavelength 350.67nm with excitation energy 3.5356 eV obtained at TD–DFT method is close to the electronic transition from the HOMO to LUMO with energy gab 4.0898eV.

Table 3: The UV–vis absorption wavelength, excitation energy and oscillator strength of GKW

Experimental [25] λ_{max}(nm) measured in methanol	TD-DFT/6-311++G(d,p) level		
	λ_{max} (nm)	Oscillator strength	E(eV)
333	350.67	0.3188	3.5356
300	313.44	0.4417	3.9556
267	295.20	0.0040	4.2000

3.5. Molecular Electrostatic Potential (MEP) analysis

Molecular electrostatic potential (MEP) affects the whole behavior of a target molecule and hence it is a very useful parameter in structural biology to understand the correlation between ligand-substrate interactions [27]. MEP surface of the GKW computed at B3LYP/6-311G++ (d,p) basis set using Gauss view is as shown in Fig.5. The MEP value of the compound is defined by electron density with 0.001 electron/bohr [3]. The electrostatic potential surface values are represented by different colors and provides a visual representation of the chemically active sites of the compound. As seen from the MEP map of the molecule, the color codes are lie in the range between -7.309e^{-2} (deepest red) and +7.309e^{-2} (deepest blue). The maximum positive region (blue color) which preferred site for nucleophilic attack whiles the maximum negative region (red color) which preferred site for electrophilic attack. The negative potential regions are usually associated with the lone pair of electronegative oxygen atoms whereas the positive potential regions are associated with hydrogen atoms. The most electro negative charge (-0.148e) and the respective electrostatic potential (-0.0216 a.u) are associated with O25 atom of the methoxy group. Hence, it is expected that O25 atom is a suitable site for electrophilic attack. The electro-negative charge of O24 and O23 atoms are -0.220e and -0.283e respectively and the corresponding electrostatic potential values are -0.0234 a.u and -0.0414 a.u. Therefore, O23 and O24 atoms are to be considered the next candidates for electrophilic attack. Similarly, the electronegative charge of the O28 atom is -0.367e and the corresponding electrostatic potential value is -0.0531 a.u. Therefore, the electrophilic attack of the tile compound is arranged in the order of O25, O24, O23 and O28. In the similar way, the maximum positive charge 0.329e and the corresponding positive electrostatic potential 0.0728 a.u are concentrated over the H27 atom of the hydroxyl group which indicates the preferred site for nucleophilic reactivity. Also, the H26 atom of the hydroxyl group is the next comparative reactivity site for nucleophilic attack.

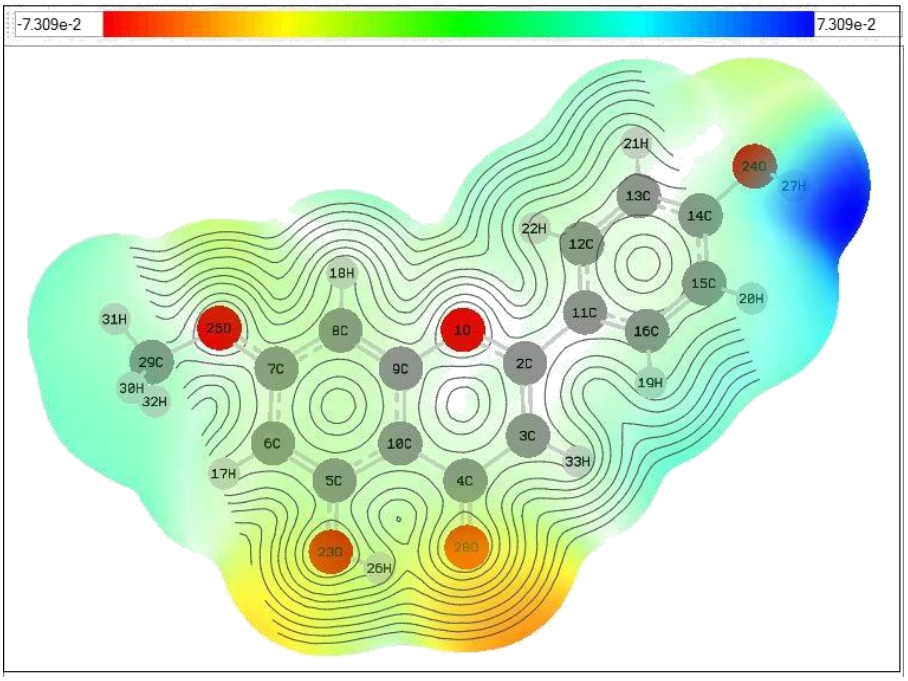

Fig. 5: MEP surface of the GKW computed at B3LYP/6-311G+ + (d,p) basis set

3.6. Molecular docking analysis

Cyclooxygenase (COX) enzyme is an integral glycoprotein membrane which catalyzes the conversion of arachidonic acid into prostaglandins (PG). The pharmacological activities of the non-steroidal anti-inflammatory drugs (NSAIDs) have been identified with concealment of prostaglandin bio synthesis and hence COX is a major target for NSAIDs in the treatment of therapeutic disease [28]. The COX enzyme exists in two isoforms, namely constitutive COX-1 and inducible COX-2. Both are identical in structure and catalytic activity, but have a few biochemical differences in the

substrate, inhibitor selectivity and in their intracellular locations [29]. COX-1 is widely distributed in all cell types to regulate the physiological processes such as gastric cytoprotection, kidney function and platelet aggregation [30]. COX-2 is expressed in several cell types, which is primarily responsible for ovulation in the birth process [31]. All the target proteins were obtained from the RCSB protein data bank (http://www.rcsb.org/pdb). The X-ray crystallographic structures of COX-1 (PDB code: 1EQG complexed with Ibuprofein and 3N8X complexed with nimesulide) and COX-2 (PDB code: 4PH9complexed with Ibuprofein and 5IKR complexed with mefenamic acid) were chosen as macro molecule. The proteins were prepared by removing the ligand while the polar hydrogen and Kollman atom charges were also added. Amino acid residues identified in the active sites of COX-1 are His90, Arg120, and Tyr355 while those of COX-2 are Arg121, Tyr356, Tyr385 and Ser530. The optimized structure of the GKW is considered as a small ligand and molecular docking was performed into the active site of COX-1 and COX-2 using Autodock 4.2 with mgltools 1.5.6 [32]. The grid maps with a grid box size of 60 x 60 x 60Å points and the grid-point spacing of 0.375Å have been used in each docking. The grid calculation was performed using Autogrid4 program implemented in Autodock and the generated box size allows the compound to rotate freely in order to find the best conformation within the target receptors. For each docking process, parameters were set to 10 automated runs for a 150 population size with a 2,500,000 maximum number of energy evaluations. Lamarckian genetic algorithm implemented in Autodock has been successfully employed to dock the compound into the active site of the COX enzymes.

3.7. Validation of docking

To validate the docking protocol, the co-crystallized ligands were removed and then re-docked it into the active sites of the particular crystal structure. The docked positions were compared to the crystal structure position by calculating root mean square deviation (RMSD) value. The RMSD value is used as a criterion for cluster analysis of the docking results. Its value depends up on the binding energy between protein and ligand. The RMSD tolerance for each docking was set as 2.0Å [33] and the resulted RMSD values were in the range of 0.59-1.01Å. This indicated that the parameter set for docking was suitable for reproducing the X-ray structure [34]. The re-docked ligands were then superimposed with the co-crystallized ligands as shown in Fig. 6. The co-crystallized ligands, binding energy and their interacting amino acid residues have been listed out in Table 4.

Table 4: Validation docking score of known inhibitors

Name of the Target & PDB ID	Known inhibitors	RMSD(Å)	Docking score kcal/mol	Interacting Amino acids
COX-1(1EQG)	Ibuprofen	0.96	-8.49	Arg120 Tyr355
COX-1(3N8X)	Nimesulide	1.01	-8.49	Arg120, Tyr355
COX-2(4PH9)	Ibuprofen	0.75	-8.81	Arg121, Tyr356
COX-2(5IKR)	Mefenamic acid	0.59	-7.80	Tyr385, Ser530

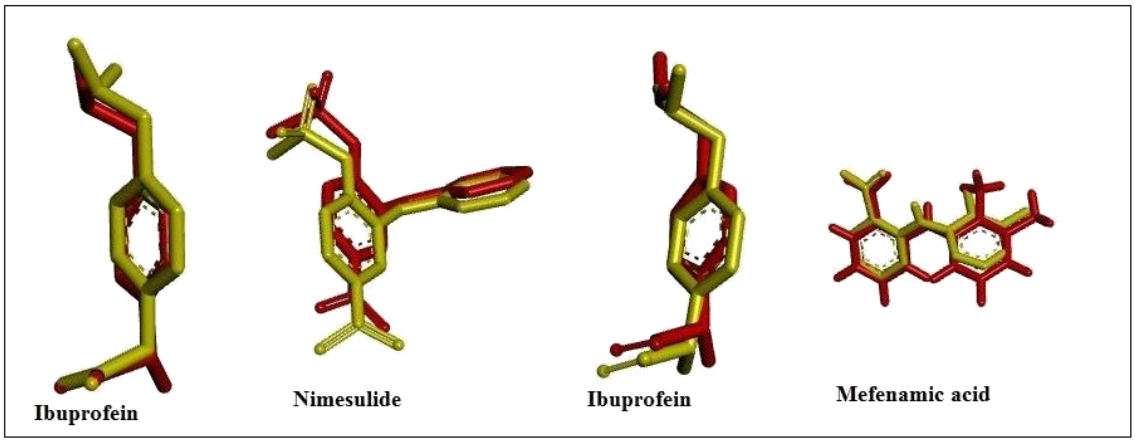

Fig. 6: Validation of docking. The red structure represents the co-crystallized ligand while the yellow structures represent the docked ligand

Fig. 7 (1EQG), 8(3N8X), 9(4PH9) and 10 (5IKR) shows the docked conformation and hydrogen-bonding interactions of GKW with the active site residues of amino acids. The binding energy and hydrogen bond interaction formed between the GKW and active site residues of the target protein COX-1 and COX-2 are listed in Table 5.

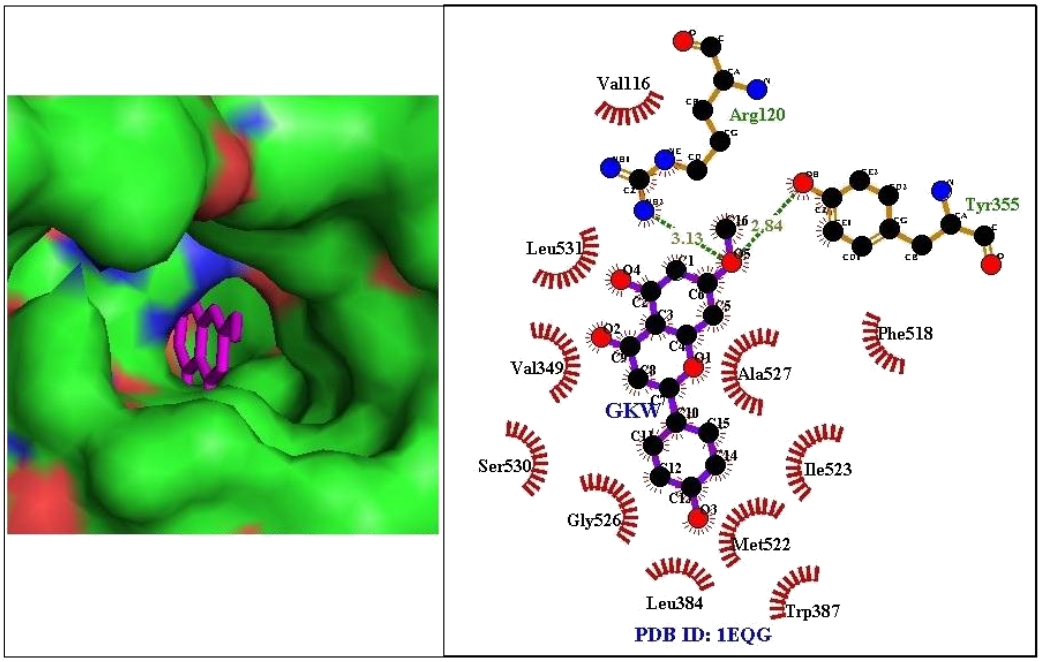

Fig. 7: The docking pose and hydrogen bond interactions of GKW with the active site residues of COX-1(1EQG)

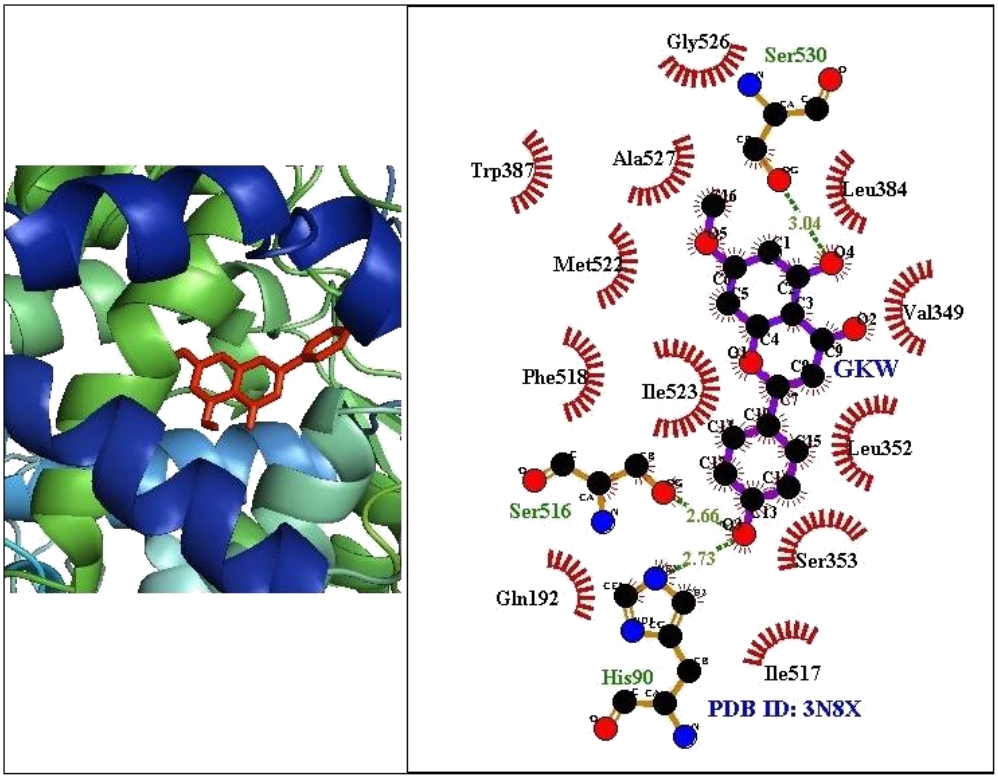

Fig. 8: The docking pose and hydrogen bond interactions of GKW with the active site residues of COX-1(3N8X)

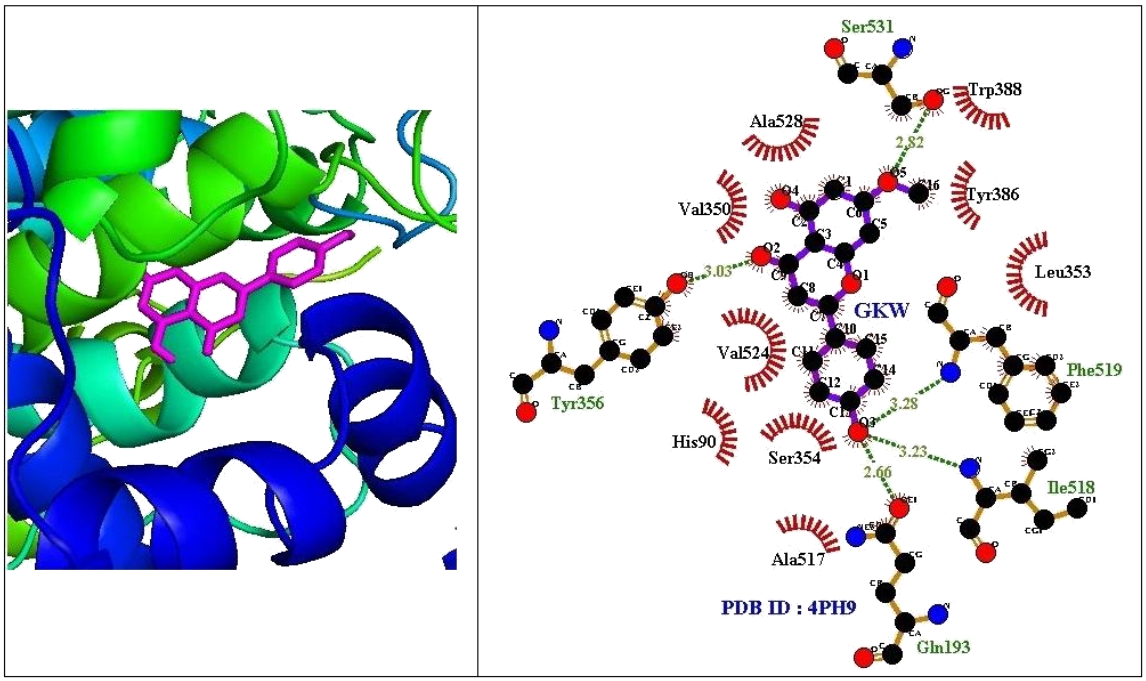

Fig. 9: The docking pose and hydrogen bond interactions of GKW with the active site residues of COX-2(4PH9)

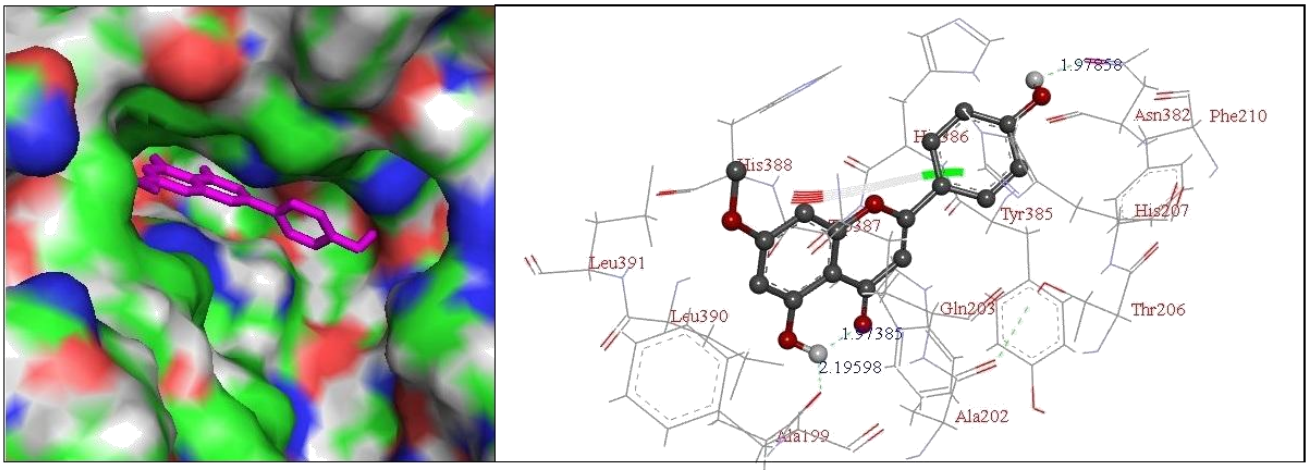

Fig. 10: The docking pose and hydrogen bond interactions of GKW with the active site residues of COX-2 (5IKR)

When analyzing the docking results, the chosen compound shows minimum bind- ing energies in the range of -8.49 to -9.34kcal/mol and it was found to be less when compared with the known standard drugs like Ibuprofen, Nimesulide and Mefenamic acid. The minimum binding energy of the docked conformation indicates the better interaction of the inhibitor with the target protein. GKW occupies binding pockets of target protein by making inter-molecular hydrogen bond interaction. Fig.7. revealed that the compound shows two hydrogen bond interactions with the residues Arg120 and Tyr355 in COX-1(1EQG), which are similar with that of Ibuprofein (Table 4). There are three hydrogen bond interaction were formed between GKW and the amino acids Ser516, His90 and Ser530 (Fig. 8) in the active sites of COX-1(3N8X). In COX-2 (4PH9), the compound shows five hydrogen bonding interaction with the amino acids Tyr356, Gln193, Ile518, Phe519 and Ser531 (Fig. 9) and these results are consistent with those reported in literature [35]. In the active sites of COX-2(5IKR), the title compound shows two H-bond interactions with the amino acids Asn382 and Ala199

(Fig. 10). The amino acids residues which involve hydrogen bond interaction with GKW are agree with that of synthetic COX-1 and COX-2 inhibitors previously reported in the literature [36, 37]. Molecular docking study reveals that GKW is docked into the active sites of the COX-1 and COX-2, the H27 atom forms inter-molecular hydrogen bond interactions with amino acids His90 (3N8X), Asn 382 (5IKR) and Gln 193 (4PH9). In addition, the H26 atom is also interacts with amino acid residues of Ala199 (5IKR) at a distance 2.195Å. Furthermore, it is interesting to note that the O25 atom of the methoxy group involves inter-molecular hydrogen bond interactions with Arg120 (1EQG), Tyr 355(1EQG) and Ser 531(4PH9). Similarly, the O23 and O28 atoms are also interact with amino acids Ser 530(3N8X) and Tyr 356(4PH9) at a distance 3.044Å and 3.027Å respectively. Besides, the O24 atom also interacts by hydrogen bond with amino acids Ser 516(3N8X), Ile 518(4PH9) and Phe 519(4PH9). Therefore, it was noticeable from our molecular docking study that the identified electrophilic and nucleophilic sites are effectively involved inter-molecular hydrogen bond interaction with the target protein and a good correlation is observed with the information provided by molecular docking study.

Table 5: The predicted Binding energies, Inhibition constant and H-bond analysis of GKW with the target proteins COX-1 and COX-2

Name of the Target protein	Donor atom	Acceptor atom	Hydrogn bond distance (Å)	Estimated Inhibition constant(Ki) nM	Binding Energy(BE) kcal/mol
COX-1 (PDB ID :1EQG)	Arg120:NH2	Ligand : O25	3.131	561.23	-8.53
	Try 355:OH	Ligand : O25	2.835		
COX-1 (PDB ID :3N8X)	Ser 516:OG	Ligand : O24	2.661	143.24	-9.34
	Ser 530:OG	Ligand : O23	3.044		
	Ligand:H27	His90:N	2.206		
COX-2 (PDB ID :4PH9)	Tyr 356:OH	Ligand : O28	3.027	349.02	-8.81
	Ser 531:OG	Ligand : O25	2.818		
	Ile 518:N	Ligand : O24	3.232		
	Phe 519:N	Ligand : O24	3.281		
	Ligand:H27	Gln193: OE1	2.660		
COX-2 (PDB ID :5IKR)	Ligand:H27	Asn 382: O	1.978	457.27	-8.65
	Ligand:H26	Ala 199: O	2.195		

4. CONCLUSION

In the present work the structural and vibrational analysis of the GKW were investigated by experimental FT-IR, FT-Raman measurements and Ab-initio HF and B3LYP methods with 6-311++G (d, p) basis set. The consistency between the calculated and experimental values indicates that the B3LYP method can generate reliable geometry and related properties of the compound. The intra-molecular hydrogen bond interaction within the molecule has been obtained at HF and B3LYP levels of theory and its effect on structural parameters were discussed. The chemical reactivity sites of the compound have been obtained by mapping electrostatic potential surface on the electron density isosurface. Remarkably, molecular docking study revealed that the chosen compound GKW interacts well with human COX-1 and COX-2 enzyme with minimum binding energy than the standard non-steroidal anti-inflammatory drugs (Ibuprofen, Nimesulide and Mefenamic acid). The inter-molecular hydrogen bond interactions between the compound and the target protein have been studied and the results were correlated well with that of electrophilic and nucleophilic reactive sites identified by the molecular electrostatic potential analysis. From this work it has been concluded that the compound under the study has significant inhibitory effect against cyclooxygenase enzymes and hence these findings will be helpful for researchers in clinical trials to synthesize and analyze a novel anti-inflammatory drug in future.

5. ACKNOWLEDGMENTS

The authors are thankful to Sophisticated Analytical Instrumentation Facility (SAIF), IIT Madras for FT-Raman studies.

6. **REFERENCES**

1. Touil YS, Arlette Fellous, Scherman D, Chabot Guy G. *Nutr. Cancer*, 2009; **61:**310-321.
2. Altinier G, Sosa S, Aquino RP, Mencherini T et al. *J Agric Food Chem,* 2007; **55:**17181723.
3. Gao Y, Liu F, Fang L, Cai R et al. *PLoS One,* 2014; **9:**e96741.
4. Kim AR, Zou YN, Park TH, Shim KH et al. *Phytother Res*, 2004; **18:** 1-7.
5. Suh N, Luyengi L, Fong HH, Kinghorn AD et al.. *Anticancer Res*, 1995; **15:**233-239.
6. Cottiglia F, Loy G, Garau D, Floris C et al. *Phytomedicine*, 2001; **8:**302-305.
7. Kraft C, Jenett-Siems K, Siems K, Jakupovic J et al. *Phytother Res*, 2003; **17:**123-128.
8. Han M, Yu X, Guo Y, Wang Y et al. *Colloids Surf B Biointerfaces,* 2014; **116:**114-120.
9. Das S, Suresh PK. *Nanomedicine* , 2011; **7:** 242- 247.
10. Abraham JP, Joe IH, George V, Nielsen OF et al. *Spectrochim. Acta A Mol Biomol Spectrosc,*2003; **59:** 193-199.
11. Sebstian S, Sundaragnesan N, Manoharan S. *Spectrochim. Acta A Mol Biomol Spectrosc,* 2009; *74***:** 312-323.
12. Frisch MJ, Trucks GW, Schlegel HB, Scuseria GE et al. *Gaussian 09, Revision A 02, Gaussian Inc Wallingford CT*, 2009.
13. Frisch A, Neilson AB, Holder AJ, *GAUSSVIEW user Manual Gaussian Inc,*Pittsburgh, CT, 2009.
14. Jamroz MH, *Vibrational Energy Distribution Analysis: VEDA 4 Computer Program,* Poland, 174-182, 2004.
15. Brito I, Brquez J, Simirgiotis M, Crdenas A et al. *Acta Cryst*, 2012; **E68:**o32-o33.
16. Sadasivam K, Kumaresan R. *Mol. Phys*, 2011; **109:**839-852.
17. Sundaraganesan N, Mariappan G, Manoharan S. *Spectrochimica Acta Part A: Molecular and Biomolecular Spectroscopy,* 2012; **87:**67-76.
18. Mariappan G, Sundaraganesan N, Manoharan S. *Spectrochimica Acta Part A: Molecular and Biomolecular Spectroscopy*, 2012; **95:**86-99.
19. Madivanane R, Harikrishnan A. *IJSRR*, 2018; **7:**619-641.
20. Kalsi PS, Spectroscopy of Organic Compounds. New Age International (P) Limited Publishers, New York, 2009.
21. Unsalan O, Yusuf Erdogdu Y, Gulluoglub MT. *J Raman Spectroscoy,* 2009; **40:** 562-570.
22. Harikrishnan Angamuthu, Madivanane Ramachandrane. *J Mol Recognit*, 2020; **33:** e2819.
23. Humberto Mendoza HL, Rios RCH. *J. Mex. Chem. Soc*, 2011**; 55:** 142-147.
24. Pearson R. *J. Org. Chem*, 1989; **54:**1423-1430.
25. Ayatollahi SA, Shojaii A, Kobarfard F, Mohammadzadeh M et al. IJPR, 2009; **8:**179-184.
26. Zsila F, Bikádi Z, Simonyi M. *Biochem Pharmacol*, 2003; **65:** 447-456.
27. Scrocco E, Tomasi J. The electrostatic molecular potential as a tool for the interpretation of molecular properties. In New concepts II, Springer Berlin Heidelberg, 1973.
28. Vane JR. *Nat. New Biol*, 1971; **231:**232-235.
29. Otto JC, Smith WL. *J. Lipid Mediat. Cell Signal*, 1995; **12:**139-156.
30. Noble SL, King DS, Olutade JI. *Am. Family Phys*, 2000; **61:** 3669-3676.
31. Gibb W, Sun M. *J Endocrinology*, 1996; **150:**497-503.
32. Huey R, Morris GM, Using AutoDock 4 with AutoDocktools: a tutorial. La Jolla, CA, USA, The Scripps Research Institute, Molecular Graphics Laboratory, 54-56,2008.
33. Kramer B, Rarey M, Lengauer T. *Proteins*, 1999; **37:**228-241.
34. Brenk R, Vetter SW, Boyce SE, Goodin DB et al. *J Mol Biol*, 2006; **357:**1449-1470.
35. Llorens O, Perez J, Palomer A, Mauleon D et al. *Journal of Molecular Graphics and Modelling*, 2002; **20:**359-371.
36. Price MLP, Jorgensen WL. *Bioorg. Med. Chem. Lett.*, 2001; **11:**1541-1544.
37. Kiefer JR, Pawlitz JL, Moreland KT, Stageman RA et al. *Nature*, 2000; **405:**97-101.